The Astrophysical Journal Letters, 971:L3 (7pp), 2024 August 10 https://doi.org/10.3847/2041-8213/ad62f6

Study of a Red Clump Giant, KIC 11087027, with High Rotation and Strong Infrared Excess—Evidence of Tidal Interaction for High Lithium Abundance

Raghubar Singh[1], Anohita Mallick[2,3], Bacham E. Reddy[2], Jeewan C. Pandey[4], and Gang Zhao[1]
[1] National Astronomical Observatories, Chinese Academy of Sciences, 20A Datun Road, Chaoyang District, Beijing 100101, People's Republic of China; raghubar@bao.ac.cn, gzhao@nao.cas.cn
[2] Indian Institute of Astrophysics, 560034, 100ft Road Koramangala, Bangalore, India
[3] Pondicherry University, R. V. Nagara, Kala Pet, 605014, Puducherry, India
[4] Aryabhatta Research Institute of Observational Sciences (ARIES), Manora Peak, Nainital 263001, India
Received 2024 May 28; revised 2024 July 4; accepted 2024 July 11; published 2024 July 31

Abstract

This Letter presents results from Kepler photometric light curves and a high-resolution spectroscopic study of a super-Li-rich giant KIC11087027. Using the light-curve analysis, we measured the star's rotational period $P_{\rm rot} = 30.4 \pm 0.1$ days, which translates to rotational velocity $V_{\rm rot} = 19.5 \pm 1.7\,{\rm km\,s^{-1}}$. The star's location in the Hertzsprung–Russell diagram, derived values of $^{12}{\rm C}/^{13}{\rm C} = 7 \pm 1$ and $[{\rm C/N}] = -0.95 \pm 0.2$, and the inferred asteroseismic parameters from secondary calibration based on spectra suggest the star is a low-mass red clump giant in the He-core burning phase. Using Gaia data, we found evidence of variation in radial velocity and proper motion, indicative of presence of an unresolved binary. The large $V_{\rm rot}$ is probably a result of tidal synchronization combined with the aftereffects of He flash, in which the size of the star is reduced significantly. The simultaneous presence of features like high rotation, very high Li abundance, strong dust shell, and strong flares in a single star is relatively uncommon, suggesting that the star experiencing tidal synchronization has recently undergone He flash. The results pose a question whether the binary interaction, hence the high rotation, is a prerequisite for the dredging up of the high amounts of Li from the interior to the photosphere during or immediately after the He-flash event.

Unified Astronomy Thesaurus concepts: Low mass stars (2050); Stellar rotation (1629); Stellar flares (1603); Asteroseismology (73); Stellar abundances (1577)

1. Introduction

A small group of red giants show very high Li abundances contrary to the general understanding that the Li gets destroyed in stars. This has been an anomaly ever since the discovery of the Li-rich giant by Wallerstein & Sneden (1982). Recent studies demonstrated that high lithium abundance among red clump (RC) giants is common (Kumar et al. 2020) and showed that the He-flash event, immediately preceding the RC, holds the key for Li enhancement (Kumar et al. 2011; Casey et al. 2019; Deepak 2019; Singh et al. 2019; Yan et al. 2021). The average Li abundance of RC giants, post He flash, is about a factor of 40 more than their counterparts on the upper red giant branch (RGB), closer to the RGB tip (Kumar et al. 2020). In addition, the study by Singh et al. (2021) showed that A(Li) evolves with the g-mode period-spacing ($\Delta\Pi_1$) evolution. During the transition phase from the degenerate-core to the convective-core He burning, the ($\Delta\Pi_1$) value increases. As a result, very high A(Li) values are mostly seen at relatively lower ($\Delta\Pi_1$) values, i.e., immediately after the He flash. The normal Li RC giants are seen at high $\Delta\Pi_1$ values. From this, they hypothesized that the super-Li-rich (SLR) giant phase (A(Li)>3.2 dex)[5] is a short-lived phenomenon, and giants with very high Li abundance have undergone Li enhancement very recently, suggesting the He flash as the source of Li enhancement. Further, the study by Mallick et al. (2023) showed the occurrence of Li-rich giants only among low-mass ($M \leqslant 2M_{\odot}$) giants and none among intermediate-mass ($M > 2M_{\odot}$) RC giants, providing indirect evidence that Li enhancement occurs during the He flash as the He flash was expected to happen in only low-mass giants (Miller Bertolami et al. 2020). We also note that there are Li abundance studies among cluster giants. Some of the SLR giants in the clusters are found to be on the RGB (Sanna et al. 2020; Nagarajan et al. 2023; Tsantaki et al. 2023). If these giants are indeed ascending the RGB for the first time, then there may be multiple ways for giants to become Li rich.

However, it is not understood what physical mechanism is responsible for the production and transportation of Li to the photosphere. Recent attempts to explain the physical process include internal gravity waves generated during the He flash (e.g., Schwab 2020; Jermyn & Fuller 2022) and thermohaline mixing (Gao et al. 2022). There are proposals in literature to drive the convection and mixing of A(Li) with the upper atmospheres, like the differential rotation due to faster core rotation (Simon & Drake 1989; Fekel & Balachandran 1993). Stars may get faster rotations due to tidal interaction in binary systems driving the desired mixing process (Denissenkov & Herwig 2004; Casey et al. 2019). Any external events like mergers or tidal interactions with companions may spin up the star, generating a strong magnetic field and creating circumstellar envelopes. One would expect all or most of these features if the Li enhancement occurred recently due to external events like mergers.

In this Letter, we analyzed high-resolution spectra of KIC11087027 for the first time. The star is an SLR giant with features such as high rotation, infrared (IR) excess, and high chromospheric activity, indicating some recent binary interaction.

[5] $A({\rm Li}) = 12 + \log\left(\frac{\rm N(Li)}{\rm (N(H)}\right)$.

2. Observations and Data Reduction

KIC11087027 was found in the sample of 12,500 stars common in the LAMOST (Zhao et al. 2006; Cui et al. 2012; Zhao et al. 2012) and Kepler (Borucki et al. 2010) fields studied by Singh et al. (2019). This star was excluded in Singh et al. (2019) because of the absence of oscillation modes in the Kepler power density spectra (PDS). The star has peculiar features like the presence of rotational modulation, flares, and IR excess. To supplement the photometric data, we obtained high-resolution ($R = 60{,}000$) optical spectra using the 2.0 m Hanle Chandra Telescope (HCT) equipped with Hanle Echelle Spectrograph (HESP)[6] for abundance analysis. We took three frames, each with a 40 minute exposure. The spectra cover the wavelength range from 3700 to 9300 Å. We obtained calibration image frames—bias, flat, and Th-Ar lamp for wavelength calibration. We also obtained high-rotation hot star spectra for removing telluric lines. We followed the standard data reduction procedure for echelle spectral reduction using IRAF.[7] The resultant spectral image has a signal-to-noise ratio (SNR) of 86. The extracted spectrum was wavelength calibrated and continuum fitted for further analysis and derivation of stellar atmospheric parameters and elemental abundances.

3. Analysis and Results

3.1. Stellar Parameters and Abundances

Stellar parameters ($T_{\rm eff}$, $\log g$, [Fe/H], $V\sin i$, and $\xi_{\rm t}$; see Table 1) are derived from high-resolution spectra. We used FASMA[8] code (Tsantaki et al. 2018) for spectrum synthesis to derive stellar parameters. The star's luminosity is derived using the Gaia Gmag (Gaia Collaboration et al. 2016, 2018) with appropriate bolometric correction (Andrae et al. 2018) and the parallax given in Gaia. The extinction coefficient in G band, $A_{\rm G}$, is calculated by the *dustapprox* code (Fouesneau et al. 2022).[9] The observed heliocentric radial velocity is derived by cross-correlating the continuum-fitted spectra with the template spectra of Arcturus.

Elemental abundances and carbon isotopic ratio are derived by matching the predicted spectra with the observed ones. Model spectra are produced using the local thermodynamic equilibrium (LTE) stellar atmospheric models (Castelli & Kurucz 2003) and the 1D radiative transfer code MOOG (Sneden 1973). The atomic and molecular line list is taken from Linemake[10] code (Placco et al. 2021). LTE Li abundance measured from the Li resonance line at 6707.78 Å is $A(\rm Li) = 4.35 \pm 0.10$ dex and from the subordinate line at 6103 Å is $A(\rm Li) = 3.85 \pm 0.1$ dex. The Li abundance is corrected for non-LTE (NLTE) effects by following correction values provided by Lind et al. (2009; Table 1). Carbon abundance is derived from atomic carbon lines at 5086 and 5384.3 Å, whereas the nitrogen abundance is derived from the $^{12}C^{14}N$ molecular line at 6486.4 Å. The carbon isotopic ratio is measured from the $^{13}C^{14}N$ molecular line in the red band of the spectra at 8004.72 Å. Errors in Li abundance and carbon isotopic ratio are derived as the quadratic sum of uncertainties in stellar parameters ($T_{\rm eff}$, $\log g$, [Fe/H], and $\xi_{\rm t}$) and SNR. Abundances of other elements are derived using equivalent widths.

Table 1
Stellar Parameters of KIC11087027

Name	KIC11087027	Reference
R.A.	19:33:14.212	...
decl.	+48:41:50.83	...
V (mag)	11.23 ± 0.09	APASS
$A_{\rm G}$ (mag)	0.11	This work
Parallax (mas)	0.86 ± 0.05	Gaia DR3
RUWE	4.38	Gaia DR3
$P_{\rm rot}$ (day)	30.38 ± 0.12	This work
$V_{\rm rot}$ (km s^{-1})	19.5	This work
$V\sin i$ (km s^{-1})	10.1 ± 0.2	This work
Inclination angle	35°	This work
Number of flares	15	This work
$T_{\rm eff}$ (K)	4920 ± 60	This work
$\log g$	2.64 ± 0.05	This work
[Fe/H]	-0.54 ± 0.05	This work
ξ_t (km s^{-1})	0.95 ± 0.05	This work
$\log(L/L_{\odot})$	1.77 ± 0.05	This work
Mass ($M_{\odot}$)	1.014 ± 0.2	This work
Radius ($R_{\odot}$)	11.69 ± 1	This work
$\rm RV_{Gaia}$ (km s^{-1})	26.70 ± 0.38	Gaia DR3
$\rm RV_{LAMOST}$ (km s^{-1})	22.71 ± 4.11	LAMOST DR7
$\rm RV_{HESP,\ Helio}$ (km s^{-1})	19.98 ± 0.26	This work
$A(\rm Li)_{NLTE}$(6103 Å)	3.95 ± 0.1	This work
$A(\rm Li)_{NLTE}$(6707 Å)	3.85 ± 0.1	This work
[C I/Fe]	-0.18 ± 0.1	This work
[N I/Fe]	0.77 ± 0.2	This work
[Na I/Fe]	0.01 ± 0.15	This work
[Mg I/Fe]	0.03 ± 0.05	This work
[Al I/Fe]	0.01 ± 0.25	This work
[S II/Fe]	-0.02 ± 0.3	This work
[Ca I/Fe]	-0.03 ± 0.3	This work
[Sc II/Fe]	-0.09 ± 0.1	This work
[Ti II/Fe]	0.0 ± 0.1	This work
[V I/Fe]	0.13 ± 0.22	This work
[Cr I/Fe]	-0.02 ± 0.3	This work
[Co I/Fe]	-0.28 ± 0.18	This work
[Ni I/Fe]	-0.34 ± 0.21	This work
[Zn I/Fe]	0.23 ± 0.2	This work
[Sr I/Fe]	-0.51 ± 0.2	This work
[Ba II/Fe]	0.04 ± 0.06	This work
[Nd II/Fe]	0.22 ± 0.1	This work
[Eu II/Fe]	0.15 ± 0.08	This work
$^{12}C/^{13}C$	7 ± 1	This work

Note. Elemental abundance w.r.t. to the Sun from Asplund et al. (2009).

3.2. Evolutionary Phase

The evolutionary phase of a star is determined using the star's location in the Hertzsprung–Russell (H-R) diagram combined with evolutionary tracks and using abundance ratios [C/N] and $^{12}C/^{13}C$. As shown in Figure 1, the star's luminosity and $T_{\rm eff}$ place it in a region in the H-R diagram that overlaps with the RC region. Similarly, observed $[\rm C/N] = -0.95 \pm 0.22$ and $[\rm Fe/H] = -0.55 \pm 0.05$ locate KIC11087027 in the RC region in the [C/N] versus [Fe/H] diagram (see Figure 5, top panel, in Hawkins et al. 2018). The very low value of $^{12}C/^{13}C = 7 \pm 1$ suggests that the star is highly evolved and, at least, beyond the luminosity bump. Though we have Kepler photometric data for

[6] https://www.iiap.res.in/centers/iao/facilities/hct/hesp/
[7] https://iraf-community.github.io/
[8] https://github.com/MariaTsantaki/fasma-synthesis
[9] https://mfouesneau.github.io/dustapprox
[10] https://github.com/vmplacco/linemake

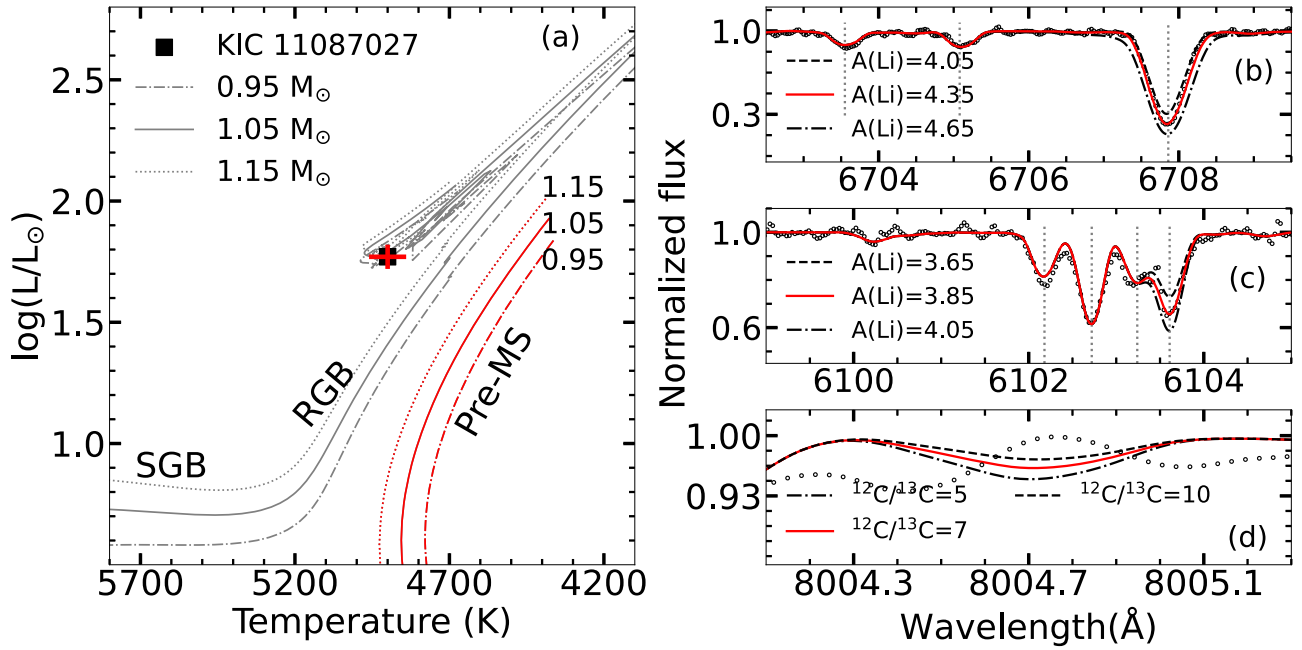

Figure 1. (a) Location of KIC11087027 (solid square) in the H-R diagram along with MESA-MIST (Paxton et al. 2011; Dotter 2016) evolutionary tracks for [Fe/H] = −0.55 dex with different masses. Panels (b), (c), and (d) are the spectral synthesis of Li resonance lines at 6707 Å, Li subordinate line at 6103 Å, and CN red line band near 8004 Å, respectively.

18 quarters, the PDS of KIC11087027 shown in Figure 2(b) do not show Gaussian power excess with oscillation modes. The inhibition of oscillation modes is caused by enhanced magnetic activity (Chaplin et al. 2011; Gaulme et al. 2014). As a result, we resorted to adopting asteroseismic parameters using secondary calibrations by Wang et al. (2023) who have derived $\Delta\Pi_1 = 187$ s and $\Delta\nu = 4.4$ μHz using spectral indices from LAMOST spectra. The values suggest KIC11087027 is an RC giant in the He-core burning phase (Bedding et al. 2011).

3.3. Detection of Stellar Flare and Measuring Flare Energy

Stellar flares are manifestations of magnetic energy. Flares are common features among main-sequence stars but uncommon among red giants due to the reduced magnetic field. Sometimes, stellar superflares may arise in binary companions or due to recent activity with stellar companion-like planets (Cuntz et al. 2000). We have investigated long-cadence (29.4 minutes) white light photometric data from the Kepler mission obtained over 4 yr. The visual inspection of the light curve showed many fast rises and exponential decay–like profiles in amplitude, suggesting the presence of flares. We used FLATW·RM code (Vida & Roettenbacher 2018) to detect stellar flares and measure flare parameters including equivalent duration (ED) and amplitude. We discovered 15 white light flares (WLFs) in KIC11087027 of the duration of a few hours each; see Figure 2 (b). WLF energy is derived from the ED of the flare and quiescent luminosity. Quiescent luminosity in the Kepler wavelength band is measured by integrating the convolution of bolometric flux (F_λ) and Kepler response function (S_{Kp}):

$$E_{\rm flare} = 4\pi R^2 \times {\rm ED} \int_{\lambda_1}^{\lambda_2} F_\lambda {}^* S_{\rm Kp} d\lambda.$$

Here λ_1 and λ_2 are the lower and upper wavelength limits of the Kepler filter. The bolometric flux F_λ for stellar parameters is taken from VOSA[11] and Kepler response function S_{Kp} is taken from the Kepler website.[12] The energy of flares is in the range of 10^{35}–10^{37} erg, which makes KIC11087027 a superflaring star.

3.4. IR Excess and Chromospheric Activity

We looked for IR excess to understand whether the star had undergone any mass loss due to external merger events, the He-flash event, or binary interactions. We collected observed fluxes from near-UV to far-IR wave bands. The observed spectral energy distribution (SED) of KIC11087027 is shown in Figure 3(b). The observed SED is compared with the model SED of the star's derived stellar atmospheric model taken from the Kurucz grid of flux models and is constructed using VOSA.[13] The star shows significant IR excess in near-IR and far-IR wavelengths, indicating an extended circumstellar environment due to episodic mass loss. The star also shows a double-peak H_α emission profile as shown in Figure 3(a), which is asymmetric and variable, indicating the presence of chromospheric activity and mass motion in stellar atmosphere (Dupree et al. 1984).

3.5. SED Modeling

The 1D radiative code DUSTY (Ivezic et al. 1999) combined with the Kurucz model fluxes is used to derive dust parameters for a given set of atmospheric parameters and the assumed dust grain distribution. We have assumed a spherically symmetric dust shell with an oxygen-rich environment of warm silicate particles (Draine & Lee 1984) and standard Mathis–Rumpl–Nordsieck grain size distribution from Mathis et al. (1977). A model SED is computed and compared with the observed SED (normalized to K_s-band fluxes) by varying dust parameters:

[11] http://svo2.cab.inta-csic.es/svo/theory/vosa/
[12] https://keplergo.github.io/KeplerScienceWebsite/
[13] http://svo2.cab.inta-csic.es/theory/vosa/

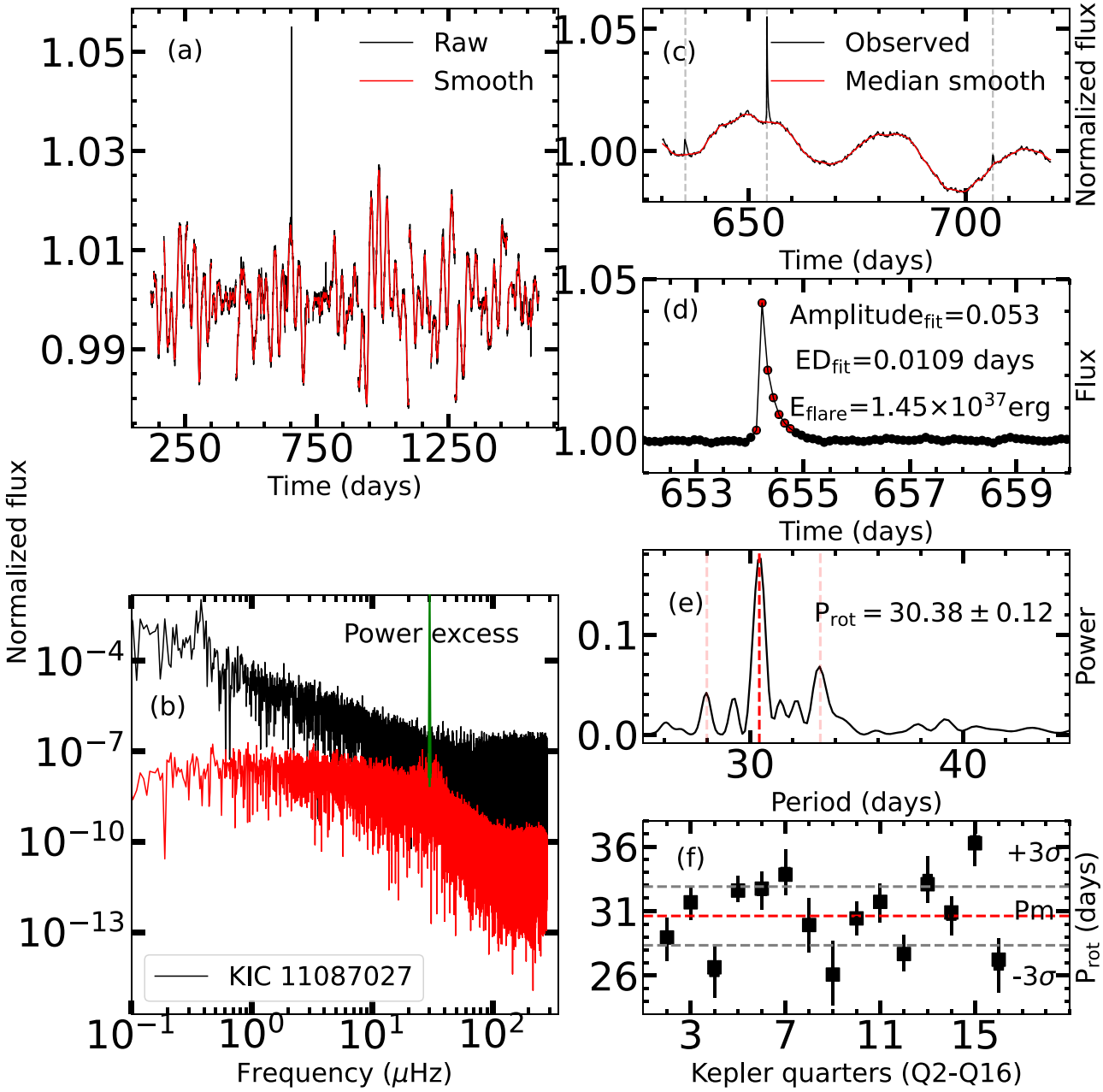

Figure 2. Kepler light-curve analysis of KIC11087027: (a) Black is a raw, and red is a median smoothed light curve. (b) Comparison of the power spectral density of KIC11087027 (black) with a similar mass star KIC12645107 (red) with no activity. (c) Seventh-quarter Kepler LC of KIC11087027, and three flares are marked. (d) The detrended light curve in the flare region and fitted flare model. Measured flare parameters are given in the figure. (e) The Lomb–Scargle periodogram of the entire 18-quarter light curve. The vertical red dashed line is measured period. (f) The rotation period measured in different quarters (Q2–Q16) gives different values.

inner dust temperature (T_{in}); optical depth (τ_ν); and dust shell relative thickness $y = \left(\frac{R_{out}}{R_{in}}\right)$.

We used a modified minimum-χ^2 test for the best fit.

$$\chi^2 = \sum\left(\frac{f_{obs} - f\ mod}{\sigma_{obs}}\right)^2 \Big/ (N - p - 1),$$

where f_{obs}, f_{mod}, and σ_{obs} are the observed flux, model flux, and error in the observed flux, respectively. (N–p–1) represents the degrees of freedom, where N is the number of observed data points and p is the number of independent parameters. Observed data are best fitted with two-component dust shells: an inner hot and an outer cooler dust shell. The two-component dust shell best-fit model using DUSTY is shown in Figure 3(b).

The dust shell inner radii and expansion velocities have been obtained using scaling relations. Other parameters of the dust shell, mass-loss rates ($\dot{M}$), kinematic age (τ_d), and total mass (M_d), are derived following Mallick et al. (2022) and are given in Table 2. The expected mass-loss rate ($\dot{M}_R$) is calculated using the modified Reimers (1975) formula for derived stellar parameters (see Table 2).

Stellar flares on a star's surface may lead to distinct inner warm and outer cool dust shells, coupled with episodic mass loss (Osten & Wolk 2015). Intense stellar radiation can lead to sublimation of dust grains closer to the star, creating an inner warm dust shell. The episodic events, shaped by flare variability, may contribute to episodic mass loss from the two dust shells.

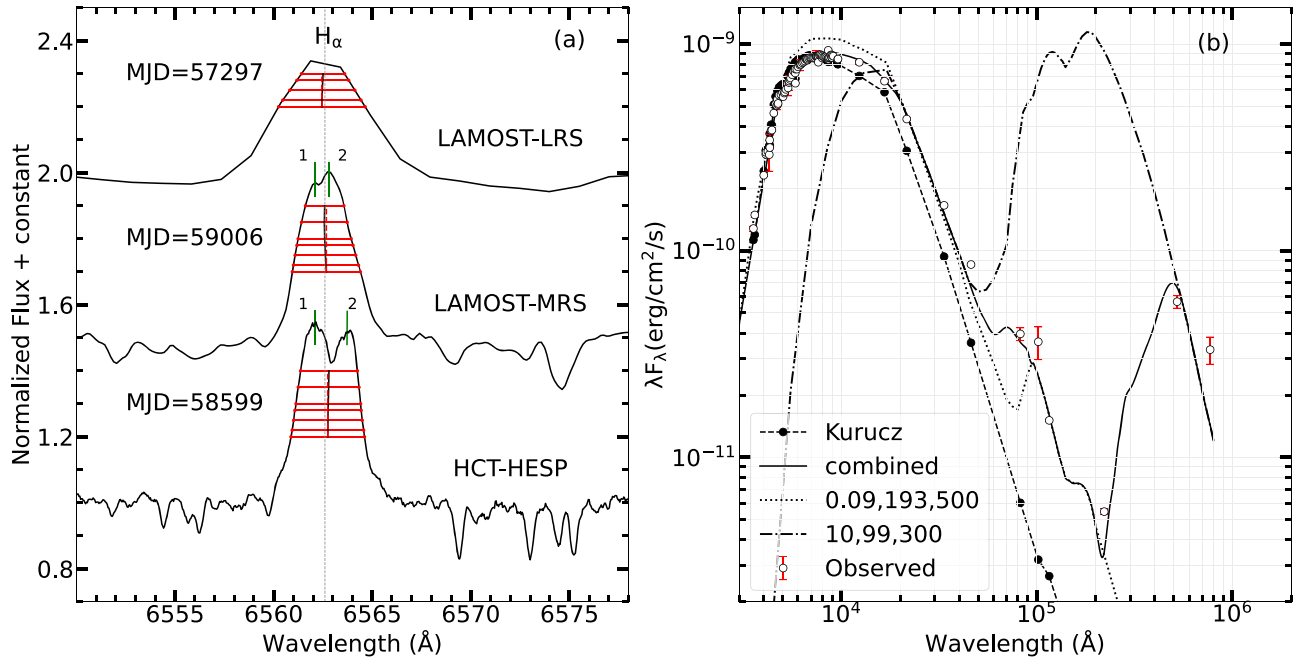

Figure 3. (a) H_α emission in KIC11087027. Three spectra are taken at different times and resolutions: LAMOST LRS ($R = 1800$), MRS, and HESP ($R = 7500$, 60,000). At higher resolution, the two H_α emission peaks become visible. (b) SED fitting to observed fluxes.

Table 2
Dust Shell Parameters of KIC11087027

	$\dot{M}_R$ (Reimer's Law) ($M_\odot$ yr^{-1})	$T_{\rm inner}$ (K)	τ_ν	$T_{\rm d}$ (K)	$V_{\rm s}$ (km s^{-1})	$R_{\rm in}$ (cm)	$t_{\rm d}$ (yr)	$\dot{M}$ (DUSTY) ($M_\odot$ yr^{-1})	$M_{\rm d}$ ($M_\odot$)
Inner Shell	...	500	0.09	193	5.48	4.87×10^{13}	2.82	5.78×10^{-9}	8.26×10^{-8}
	6.68×10^{-11}								
Outer Shell	...	300	10	99	1.41	2.45×10^{14}	55.09	8.29×10^{-7}	2.32×10^{-4}

3.6. Rotational Velocity

We estimated the star's rotational velocity, $V_{\rm rot}$, from spectra and photometric light-curve data. The observed spectral width results from the blending of other lines in the vicinity, instrumental broadening, and stellar phenomena like macroturbulence and rotation. We used two well-defined Fe I lines at 6703 and 6705 Å for extracting the rotation part of the line width by computing a set of profiles for given line abundance values, stellar parameters, and instrumental broadening as measured from the Th-Ar calibration lines in the vicinity. The macroturbulence velocity, $V_{\rm mac} = 3.9$ km s^{-1}, is calculated using calibration relation involving $T_{\rm eff}$ and $\log g$ (Hekker & Meléndez 2007). Using the χ^2 test, we found the observed profiles best fit for $V\sin i = 10.1$ km s^{-1}. We also made use of Kepler photometric data to determine the period of the star. The data showed modulation in the light curve, probably due to large stellar spots that corotate with the stellar surface. We performed a periodogram analysis by using the Lomb–Scargle method (Scargle 1982) in the Kepler data spanning 4 yr. Periods ranging from 26 to 33 days during different quarters, as shown in the bottom panel of Figure 2(f), are found. The average period is found to be 30.38 ± 0.12 days. Using the estimated star's radius, $R = 11.69 \pm 1\ R_\odot$, and considering this period as a rotational period ($P_{\rm rot}$), we found average $V_{\rm rot} = 19.5 \pm 1.7$ km s^{-1}, which is quite large for an evolved star like KIC11087027. The quarter-to-quarter variation, with a median absolute deviation of 2.1, in the rotation is probably caused by latitudinal differential rotation (Suto et al. 2022).

3.7. Binarity: Tidal Synchronization

We did not find any resolved binary of KIC11087027 within 10″ in the Gaia survey, and also, no signature of the eclipse is present in the Kepler light curve. However, the presence of any unresolved companion cannot be ruled out. The star has been observed at four different epochs in APOGEE, LAMOST, and HCT-HESP over a span of 7 yr, and we found a small difference in the radial velocity (see Table 1). Gaia astrometry has been used for detecting unresolved companions of stars within 1″, which can affect astrometric measurements. The Gaia renormalized unit weight error (RUWE) value is greater than 1.4 for the multiple system (Ziegler et al. 2020), and the RUWE of KIC11087027 is 4.38. This inflated value of RUWE indicates a close unresolved binary or multiple system, as a wide binary does not inflate RUWE. This is further supported by the proper motion anomaly found for KIC11087027. Proper motion values of KIC11087027 measured by Tycho-2 in the updated UCAC4 catalog (Zacharias et al. 2013) are $\mu_{\rm T} = (-2.1 \pm 0.7, -5.0 \pm 0.5)$ mas yr^{-1}, and in the Gaia DR3, they are $\mu_{\rm G} = (-1.547 \pm 0.067, -7.289 \pm 0.059)$ mas yr^{-1}. Significant acceleration ($\sigma = 4.55$) is found in the δ direction with $\mu_{\rm T} - \mu_{\rm G} = (-0.55 \pm 0.70, 2.29 \pm 0.50)$, a signature that the star

may be an unresolved binary or has multiple systems. The absence of oscillation modes (see Figure 2(b)) and the presence of strong magnetic activity in a low-mass fast-rotating evolved star (Gaulme et al. 2014) suggests that the star KIC11087027 is probably in a tidally synchronized system. Another evidence is the star's high projected rotational velocity ($V\sin i = 10\,\mathrm{km\,s^{-1}}$) for its color, $(B-V) = 1.04$ (De Medeiros et al. 2002). The observations suggest KIC11087027 is tidally locked with an unresolved close binary companion with an orbital period of 30.4 days.

4. Discussion

Red giants with very high Li and strong IR excess are rare because both properties seem transient and evolve differently. Though we do not have much information about IR excess, the large surveys showed no evidence of IR excess among giants (Bharat Kumar et al. 2015), and only a couple of Li-rich giants and SLRs are known to have IR excess (Mallick et al. 2022). The general lack of IR excess among Li-rich giants indicates either no ejection of mass during the event that caused Li enrichment, or mass loss occurred, but the resultant IR excess probably diluted faster than the Li depletion. In that sense, the star KIC11087027 is unusual, with very high Li and large IR excess. This suggests Li enrichment occurred recently, assuming the high Li and IR excess result from a single event that is responsible for high Li among RC giants. Further, it is demonstrated that $\Delta\Pi_1$ is a proxy to the time evolution of a degenerate core into a convective core, i.e., older RC giants with normal Li have relatively much higher $\Delta\Pi_1$ values (Singh et al. 2021). The estimated value of $\Delta\Pi_1$=187 s from spectra (Wang et al. 2023) indicates that KIC 11087027 is a young RC and Li enrichment occurred very recently. The star also shows very high stellar rotation ($V_{\rm rot} = 19.5\,\mathrm{km\,s^{-1}}$), which causes the star to have high chromospheric activity with flares. What process might have created all the above signatures in a single star is unclear. If these properties are a consequence of a single event like a He flash and evolve at different timescales, one would expect stars with all these properties to be uncommon. Here, we also note the study by Sneden et al. (2022), which shows a subtle correlation between the strength of the chromospheric line at He I 10830 Å and the high A(Li) in giants. They also show a higher binary fraction among Li-rich giants compared to Li-poor ones, implying some kind of binary interaction for Li production and chromospheric activity.

In the case of KIC11087027, we discuss two plausible scenarios. One is an in situ process in single-star evolution, and the other is the stars' binary evolution, where orbital synchronization causes high rotation, aiding high Li abundance. It is highly likely that the He flash holds the key to the high Li anomaly among RC giants (Casey et al. 2019; Deepak 2019; Singh et al. 2019, 2021; Mallick et al. 2023). Of course, we need to understand the nature of some of the very high Li-rich giants reported in clusters. These giants appear to be on the RGB and well before the RGB tip (Sanna et al. 2020; Nagarajan et al. 2023), i.e., before the He-flash event. It is important to analyze the cluster Li-rich giants using asteroseismology to find whether these are ascending the RGB. We will address this in a later study.

As per the RC Li-rich giants, the question remains about the physical process that mixes internally produced Li with the upper layers. Is the He flash the sole process? And does external aid, such as tidal locking, also play a role? Supporting the high levels of Li among RC giants, Schwab (2020) constructed models in which the powerful gravity waves generated during the He flash provide a conducive environment for large-scale convection. For this, they required the diffusion coefficient $D_{\rm mix} = 10^{11}\,\mathrm{cm^2\,s^{-1}}$, which is a few orders of magnitude more than expected in stars ascending the RGB.

Let us assume Li gets produced inside the star through the Cameron–Fowler mechanism (Cameron & Fowler 1971) and the He flash aids large-scale mixing. Though the models predict no observable feature like IR excess due to the He flash at the center, it is not unreasonable to suggest mass loss occurs due to the flash, and the severity of mass loss depends on the intensity of the He flash. The resultant IR excess is diluted faster since it is a one-time event. This may be why RC giants with IR excess are rare. Importantly, all the SLRs or Li-rich giants do not need to have IR excess as they may evolve at different timescales. The RC giants with IR excess are found more likely to be SLR or Li rich (Mallick et al. 2022), suggesting that IR excess dilutes faster than Li depletion.

Concerning the high rotational velocity of KIC11087027, it is expected that the He flash and the consequent reduction in star size by a factor of ∼10 will spin up the star. Given the $V_{\rm rot}$ $\sim$0.7 $\mathrm{km\,s^{-1}}$ for the giants at the RGB tip, one would expect $V_{\rm rot}$ ∼7 $\mathrm{km\,s^{-1}}$ for a young RC giant. This expected value, due to a sudden drop in the size of the giant from the RGB tip to the RC, is much smaller than the observed value of 19.5 $\mathrm{km\,s^{-1}}$. This implies high rotation in KIC11087027 and other Li-rich RC stars found in the literature probably arose due to external factors like mergers or tidal locking. A primary giant at or near the RGB tip, which is tidally locked with its binary star, may have a larger rotational velocity than a single star. In the case of KIC11087027, observed $V_{\rm rot} = 19.5\,\mathrm{km\,s^{-1}}$ may be the combination of tidal locking and the aftereffect of the He flash.

If we assume the star in tidal locking with a close binary has slightly more $V_{\rm rot}$, say, 2 $\mathrm{km\,s^{-1}}$ rather the expected value of 0.7 $\mathrm{km\,s^{-1}}$, the resulting post-He-flash $V_{\rm rot}$ value matches with the observed high velocity. The large $V_{\rm rot}$ will increase the diffusion coefficient to $10^{11}\,\mathrm{cm^2\,s^{-1}}$ (Casey et al. 2019) as $D_{\rm mix} \propto \Omega^2$. Models show that a significant increase in the value of $D_{\rm mix}$ may result in the observed lithium abundance in the photosphere (Denissenkov & VandenBerg 2003).

5. Conclusion

In this study, we reported results from the Kepler photometric light curve and high-resolution spectral data. Based on variation in radial velocity and Gaia astrometric data, we suggest that KIC11087027 has an unresolved companion. The observed high $V_{\rm rot} = 19.5\,\mathrm{km\,s^{-1}}$ may be a result of a combination of tidal synchronization in a binary system and the effect of the He flash. The high rotation probably results in a high diffusion coefficient, hence the high Li abundance. The presence of several transient features like very high Li abundance, multiple dust shells, high rotation, and strong flares provide evidence that either the star has undergone a merger-induced He flash (Mallick et al. 2022) or the tidally locked primary star has undergone the He flash very recently. Also, to have a comprehensive understanding of the origin of Li-enhanced giants, it is imperative to understand the nature of Li-rich giants in clusters that are reported to be ascending the RGB.

Acknowledgments

We thank the anonymous referees for useful comments that have improved our Letter. This study is supported by the National Natural Science Foundation of China under grant No. 11988101, and the National Key R&D Program of China No. 2019YFA0405500. Guoshoujing Telescope (the Large Sky Area Multi-Object Fiber Spectroscopic Telescope LAMOST) is a National Major Scientific Project built by the Chinese Academy of Sciences. LAMOST is operated and managed by the National Astronomical Observatories, Chinese Academy of Sciences. This work presents results from the European Space Agency (ESA) space mission Gaia. Gaia data are being processed by the Gaia Data Processing and Analysis Consortium (DPAC). Funding for the DPAC is provided by national institutions, in particular the institutions participating in the Gaia MultiLateral Agreement (MLA). The Gaia mission website is https://www.cosmos.esa.int/gaia. We gratefully acknowledge the entire team of Kepler space telescope which is funded by NASA's Science Mission.

ORCID iDs

Raghubar Singh https://orcid.org/0000-0001-8360-9281
Anohita Mallick https://orcid.org/0000-0002-4282-605X
Bacham E. Reddy https://orcid.org/0000-0001-9246-9743
Jeewan C. Pandey https://orcid.org/0000-0002-4331-1867
Gang Zhao https://orcid.org/0000-0002-8980-945X

References

Andrae, R., Fouesneau, M., Creevey, O., et al. 2018, A&A, 616, A8
Asplund, M., Grevesse, N., Sauval, A. J., & Scott, P. 2009, ARA&A, 47, 481
Bedding, T. R., Mosser, B., Huber, D., et al. 2011, Natur, 471, 608
Bharat Kumar, Y., Reddy, B. E., Muthumariappan, C., & Zhao, G. 2015, A&A, 577, A10
Borucki, W. J., Koch, D., Basri, G., et al. 2010, Sci, 327, 977
Cameron, A. G. W., & Fowler, W. A. 1971, ApJ, 164, 111
Casey, A. R., Ho, A. Y. Q., Ness, M., et al. 2019, ApJ, 880, 125
Castelli, F., & Kurucz, R. L. 2003, in IAU Symp. 270, Modelling of Stellar Atmospheres, ed. N. Piskunov, W. W. Weiss, & D. F. Gray (San Francisco, CA: ASP), A20
Chaplin, W. J., Bedding, T. R., Bonanno, A., et al. 2011, ApJL, 732, L5
Cui, X.-Q., Zhao, Y.-H., Chu, Y.-Q., et al. 2012, RAA, 12, 1197
Cuntz, M., Saar, S. H., & Musielak, Z. E. 2000, ApJL, 533, L151
De Medeiros, J. R., Da Silva, J. R. P., & Maia, M. R. G. 2002, ApJ, 578, 943
Deepak, R. B. E. 2019, MNRAS, 484, 2000
Denissenkov, P. A., & Herwig, F. 2004, ApJ, 612, 1081
Denissenkov, P. A., & VandenBerg, D. A. 2003, ApJ, 593, 509
Dotter, A. 2016, ApJS, 222, 8
Draine, B. T., & Lee, H. M. 1984, ApJ, 285, 89
Dupree, A. K., Hartmann, L., & Avrett, E. H. 1984, ApJL, 281, L37
Fekel, F. C., & Balachandran, S. 1993, ApJ, 403, 708
Fouesneau, M., Andrae, R., Sordo, R., & Dharmawardena, T. 2022, dustapprox, v0.1, GitHub, https://github.com/mfouesneau/dustapprox
Gaia Collaboration, Brown, A. G. A., Vallenari, A., et al. 2018, A&A, 616, A1
Gaia Collaboration, Prusti, T., de Bruijne, J. H. J., et al. 2016, A&A, 595, A1
Gao, J., Zhu, C., Yu, J., et al. 2022, A&A, 668, A126
Gaulme, P., Jackiewicz, J., Appourchaux, T., & Mosser, B. 2014, ApJ, 785, 5
Hawkins, K., Ting, Y.-S., & Walter-Rix, H. 2018, ApJ, 853, 20
Hekker, S., & Meléndez, J. 2007, A&A, 475, 1003
Ivezic, Z., Nenkova, M., & Elitzur, M. 1999, arXiv:astro-ph/9910475
Jermyn, A. S., & Fuller, J. 2022, arXiv:2206.13479
Kumar, Y. B., Reddy, B. E., Campbell, S. W., et al. 2020, NatAs, 4, 1059
Kumar, Y. B., Reddy, B. E., & Lambert, D. L. 2011, ApJL, 730, L12
Lind, K., Asplund, M., & Barklem, P. S. 2009, A&A, 503, 541
Mallick, A., Reddy, B. E., & Muthumariappan, C. 2022, MNRAS, 511, 3741
Mallick, A., Singh, R., & Reddy, B. E. 2023, ApJL, 944, L5
Mathis, J. S., Rumpl, W., & Nordsieck, K. H. 1977, ApJ, 217, 425
Miller Bertolami, M. M., Battich, T., Córsico, A. H., Christensen-Dalsgaard, J., & Althaus, L. G. 2020, NatAs, 4, 67
Nagarajan, N., Sneden, C., Afsar, M., & Pilachowski, C. 2023, AAS Meeting Abstracts, 241, 367.01
Osten, R. A., & Wolk, S. J. 2015, ApJ, 809, 79
Paxton, B., Bildsten, L., Dotter, A., et al. 2011, ApJS, 192, 3
Placco, V. M., Sneden, C., Roederer, I. U., et al. 2021, RNAAS, 5, 92
Reimers, D. 1975, MSRSL, 8, 369
Sanna, N., Franciosini, E., Pancino, E., et al. 2020, A&A, 639, L2
Scargle, J. D. 1982, ApJ, 263, 835
Schwab, J. 2020, ApJL, 901, L18
Simon, T., & Drake, S. A. 1989, ApJ, 346, 303
Singh, R., Reddy, B. E., Campbell, S. W., Kumar, Y. B., & Vrard, M. 2021, ApJL, 913, L4
Singh, R., Reddy, B. E., & Kumar, Y. B. 2019, MNRAS, 482, 3822
Sneden, C., Afşar, M., Bozkurt, Z., et al. 2022, ApJ, 940, 12
Sneden, C. A. 1973, PhD thesis, Univ. of Texas at Austin
Suto, Y., Sasaki, S., Nakagawa, Y., & Benomar, O. 2022, PASJ, 74, 857
Tsantaki, M., Andreasen, D. T., Teixeira, G. D. C., et al. 2018, MNRAS, 473, 5066
Tsantaki, M., Delgado-Mena, E., Bossini, D., et al. 2023, A&A, 674, A157
Vida, K., & Roettenbacher, R. M. 2018, A&A, 616, A163
Wallerstein, G., & Sneden, C. 1982, ApJ, 255, 577
Wang, C., Huang, Y., Zhou, Y., & Zhang, H. 2023, A&A, 675, A26
Yan, H.-L., Zhou, Y.-T., Zhang, X., et al. 2021, NatAs, 5, 86
Zacharias, N., Finch, C. T., Girard, T. M., et al. 2013, AJ, 145, 44
Zhao, G., Chen, Y.-Q., Shi, J.-R., et al. 2006, ChJAA, 6, 265
Zhao, G., Zhao, Y.-H., Chu, Y.-Q., Jing, Y.-P., & Deng, L.-C. 2012, RAA, 12, 723
Ziegler, C., Tokovinin, A., Briceño, C., et al. 2020, AJ, 159, 19